Supporting Information

Conductive behavior of cross-linked electropolymeric films formed by 'star-shaped' multifunctional precursors

Ying Wang, [a] Bohan Wang, [a] Lingyu Wang, [a] Hanlin Gan, [a] Wei Xiong, [a] Yue Yu, [a] Zhisheng Zhou, [a] Shaohua Tong, [a] Ning Li, [a] and Yuguang Ma*[a]

[a.] State Key Laboratory of Luminescent Materials and Devices, Institute of Polymer Optoelectronic Materials and Devices, South China University of Technology, Guangzhou 510640, P. R. China. Email: wangbohan@scut.edu.cn, ygma@scut.edu.cn

Table of Contents

1. TCTA electropolymerization film morphology

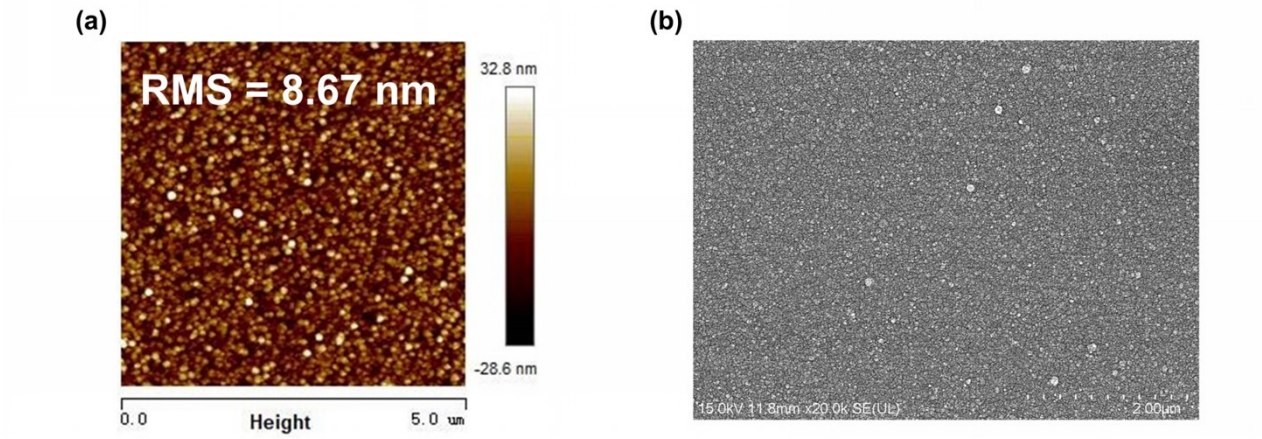

Fig. S1 (a) Atomic force microscopy image and (b) Scanning electron microscopy image of the TCTA electropolymerization film.

2. Electrochemistry of TCTA

2.1 Electropolymerization of TCTA

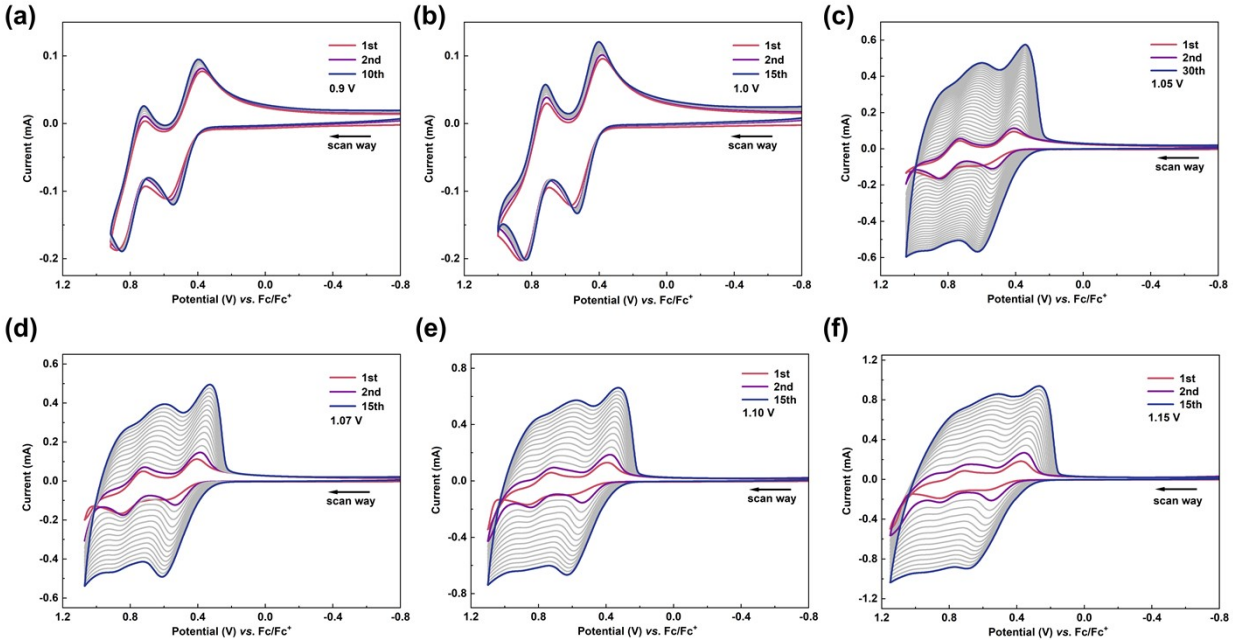

Fig. S2 CV curves of TCTA electropolymerization with various potential windows: -0.8 to (a) 0.90 V, (b) 1.00 V, (c) 1.05 V, (d) 1.07 V, (e).1.10 V, and (f) 1.15 V.

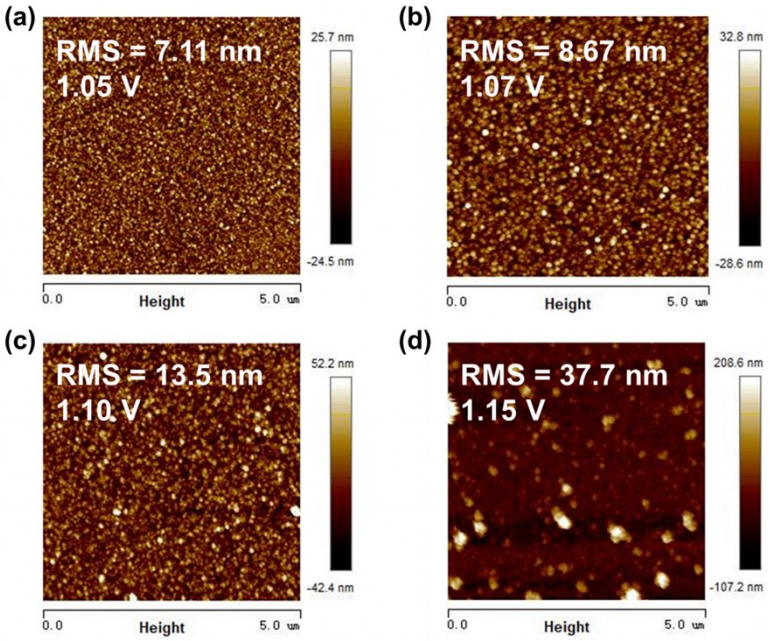

Fig. S3 AFM images of p-TCTA films prepared under different maximum applied potentials. The maximum potentials are: (a) 1.05 V, (b) 1.07 V, (c) 1.10 V, and (d) 1.15 V.

When the maximum applied potential exceeds 1 V, the CV curves of TCTA show a pronounced and continuous increase in current with successive voltammetric cycles, signaling ongoing material deposition and film growth. Finally, a clearly visible polymer film forms on the electrode. Conversely, at maximum applied potentials below 1 V, the electrode shows no significant deposits.

As shown in Fig. S3, the surface roughness of the films increases with the maximum applied potential. Although the film obtained at a maximum potential of 1.05 V exhibited the lowest RMS roughness, fine cracks were observed at the film edges. Taking all factors into account, the potential window of -0.80 to 1.07 V was selected as the optimal range for TCTA electropolymerization.

Table S1 Comparison of surface roughness of electropolymerized films

Electropolymerized film	Electrolyte	Method	Roughness/ nm	Ref.
Polythiophene	$HClO_4/H_2O$	Chronoamperometry	3.5	1
	$TBAPF_6$/ACN	Chronoamperometry	21.0	2
Polypyrrole	$LiClO_4/H_2O$	Chronoamperometry	156.7	3
	$LiClO_4$/ACN	Chronoamperometry	200.0	4
Polycarbazole	$LiClO_4$/ACN	Cyclic Voltammetry	100.0	5
Polyaniline	H_2SO_4/H_2O	Chronoamperometry	58.0	6
Poly(3,4-ethylenedioxythiophene)	$PSSNa/H_2O$	Galvanostatic	7.36	7
	$TBAClO_4$/PC	Chronoamperometry	36.00	8
Multifunctional "star-shaped" precursors				
TCPC	$TBAPF_6$/ACN/DCM	Cyclic Voltammetry	2.8	9
PFCzPO	$TBAPF_6$/ACN/DCM	Cyclic Voltammetry	3.64	10
TCBzC	$TBAAsF_6$/ACN/DCM	Cyclic Voltammetry	2.88	11
TCNzC	$TBAAsF_6$/ACN/DCM	Cyclic Voltammetry	2.76	11
p-TCTA	$TBAPF_6$/DCM/ACN/PC	Cyclic Voltammetry	8.67	**This work**

The literature survey indicates that electrochemically cross-linked polymer films derived from "star-shaped" precursors generally exhibit good surface smoothness (RMS < 10 nm) and possess very low doping levels, thereby exhibiting semiconducting behavior. In contrast, the electropolymerization of classical linear conducting polymers is typically carried out in either aqueous or organic solvent systems. Films prepared in organic solvents tend to show slightly higher surface roughness. In aqueous systems, the monomers usually require the assistance of surfactants or acids to dissolve. Some reports have shown that, with the aid of surfactants, the resulting films can achieve relatively high smoothness. However, polymer films fabricated under such conditions are typically in a doped state. Although they may exhibit good electrical conductivity, they do not possess intrinsic semiconducting properties.

2.2 Electrical analysis of TCTA

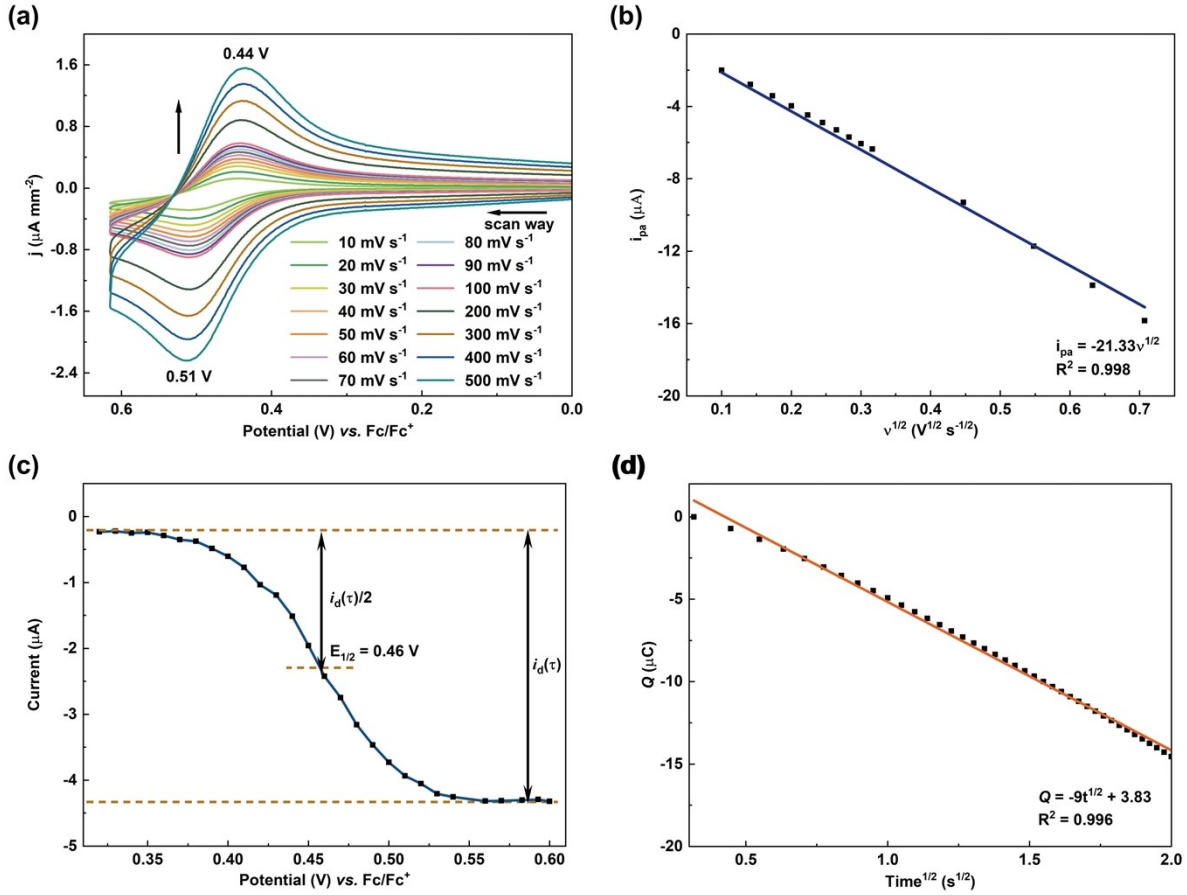

Fig. S4 (a) CV curves of TCTA at scan rates ranging from 10 to 500 mV s^{-1}. (b) The peak current of TCTA's first oxidation peak plotted as a function of the square of the scan rate. (c) Sample voltammetric curve demonstrating TCTA's electrochemical response. (d) Linear chronocoulometric plots of TCTA at 0.6 V.

The electroanalytical characterization of TCTA's first electrochemical reaction is detailed in Fig. S4. In Fig. S4a, the first electrochemical process of TCTA is shown to exhibit thermodynamically reversible CV curves, with an oxidation peak (E_{pa}) at 0.51 V and a reduction peak (E_{pc}) at 0.44 V. The peak separation is 0.07 V, and the half-wave potential ((E_{pc} + E_{pa})/2) is 0.47 V. The sample voltammetric curve (Fig. S4c) suggests that between 0.56 V and 0.6 V, TCTA undergoes its first electrochemical process governed by diffusion; the half-wave potential is 0.46 V, consistent with the CV curves. Utilizing the Randles-Sevcik equation[12] (1) and Anson's equation[13] (2), along with the fitting results from Fig. S4b and d, the electron transfer number, n, during this process is calculated to be 0.92. Consequently, the first electrochemical process of TCTA is identified as a thermodynamically reversible single-electron process.

$$i_p = 0.4463\left(\frac{F^3}{RT}\right)^{\frac{1}{2}} n^{\frac{3}{2}} A D_R^{\frac{1}{2}} C_R^* \nu^{\frac{1}{2}} \#(1)$$

$$Q = \frac{2nFAD_R^{\frac{1}{2}} C_R^* t^{\frac{1}{2}}}{\pi^{\frac{1}{2}}} + Q_{dl} + nFA\Gamma_R \#(2)$$

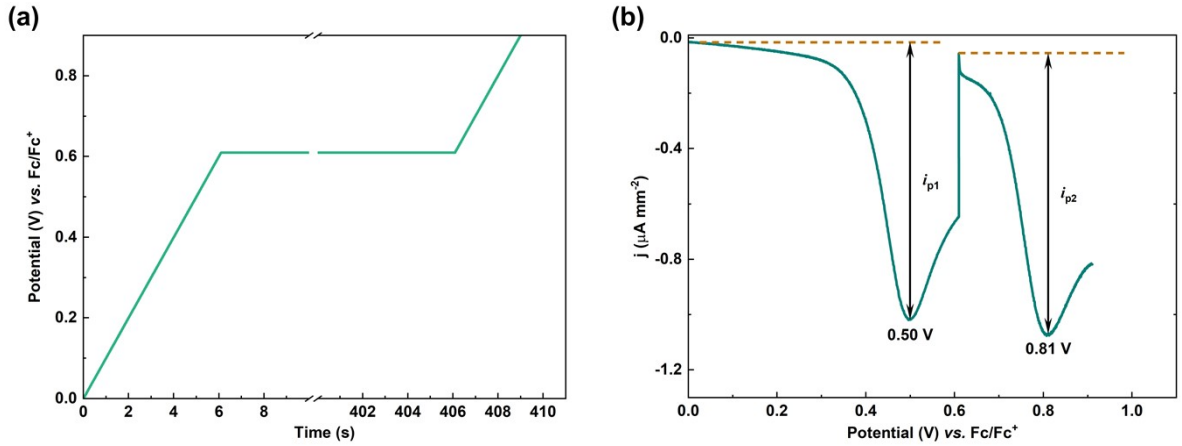

Fig. S5 Method of allowing the current of the first wave to decay before scanning the second wave. (a) Potential program with a scan rate of 100 mV s^{-1} and a decay period of 400 seconds. (b) Resulting voltammogram for TCTA.

A specialized voltammetric protocol (Fig. S5a) is utilized to explore the second electrochemical process of TCTA.[12] The procedure initiates at 0 V and progresses to 0.6 V at a scan rate of 100 mV s^{-1}. Subsequently, the potential is maintained at 0.6 V for 400 seconds to facilitate the depletion of TCTA near the electrode while preserving a steady concentration of its monovalent cations. The scan then resumes at the same rate, extending from 0.6 V to 0.9 V. According to Fig. S5b, the ratio of the peak currents, i_{p2}/i_{p1}, is 1.016, indicating that the electron transfer number in the second process mirrors that of the first. This, coupled with the CV curves, confirms that the second electrochemical process is also a thermodynamically reversible single-electron process.

3. Optical bandgap of p-TCTA

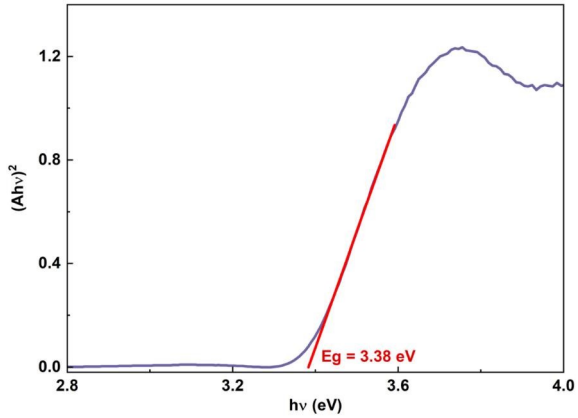

Fig. S6 Optical bandgap of p-TCTA.

4. Electrochemistry of p-TCTA

4.1 Kinetic analysis of p-TCTA

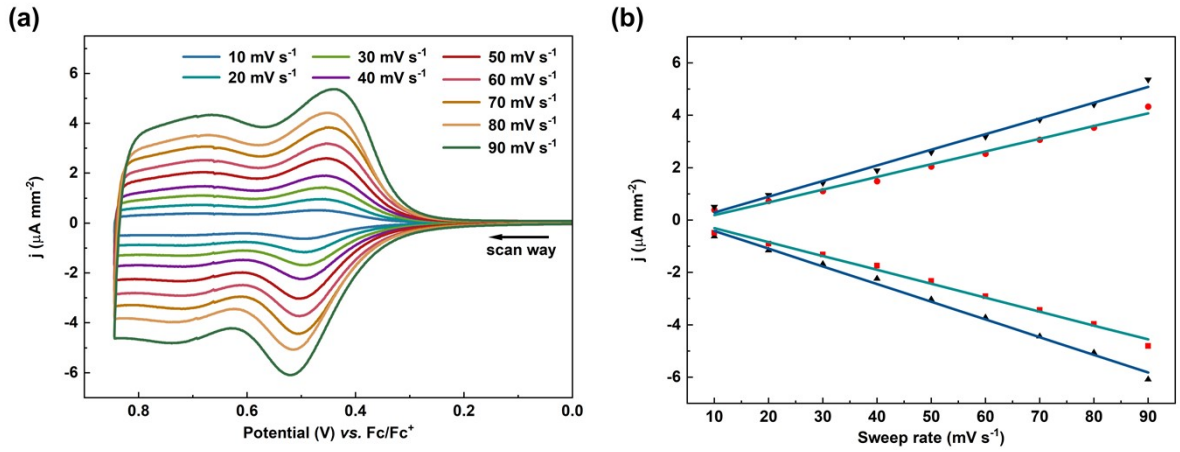

Fig. S7 (a) CV curves of p-TCTA at scan rates ranging from 10 to 90 mV s^{-1}. (b) Peak current of p-TCTA plotted as a function of scan rate.

4.2 Capacitive performance of p-TCTA and estimation of electrochemical doping charge

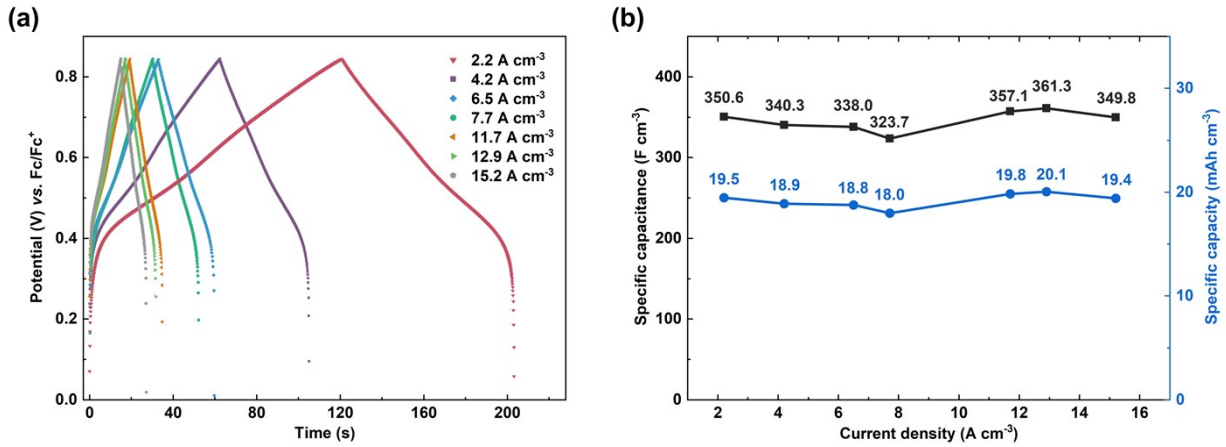

Fig. S8 (a) Galvanostatic charge/discharge profiles of p-TCTA at various current densities. (b) Specific capacitance and capacity of p-TCTA across different current densities.

According to Fig. S8, p-TCTA demonstrates a stable capacitance performance of approximately 350 F cm^{-3} under charge/discharge conditions across various current densities. This indicates that no polarization occurs during the doping process at these current densities, and the doping state of p-TCTA reflects the thermodynamic equilibrium at the corresponding measured potentials. Consequently, the doping charge at a given potential can be estimated from the constant-current charging curve, as shown in Fig. S9a. The doping charge is calculated as the Faradaic charge, obtained by subtracting the non-Faradaic charge from the total charge. Assuming all electrochemically doped charges in p-TCTA act as carriers, the carrier concentration at different doping potentials can be estimated as the ratio of the doping charge to the Faraday constant, as illustrated in Fig. S9b. This analysis further enables the estimation of the carrier mobility at various doping levels.

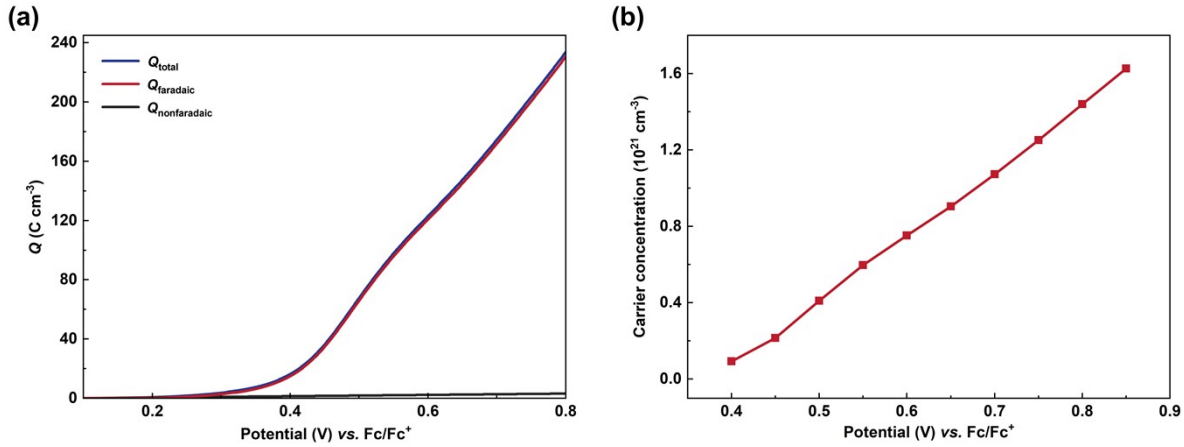

Fig. S9 (a) Total, Faradaic, and non-Faradaic charges as a function of potential. (b) Estimated carrier concentration plotted against doping potential.

Table S2 Capacitive performance of electrochemically cross-linked polymer films reported in recent years

Electropolymerized film	Current density	Specific capacitance	Ref.
P-P_{Cu}	5 A g^{-1}	332 F g^{-1}	14
P[Th_3CNTT-TPA]	3 A g^{-1}	235 F g^{-1}	15
PolyMnPor	2 A g^{-1}	250 F g^{-1}	16
Poly[Ni(salphen)]/MWCNT	0.1 mA cm^{-2}	200 F g^{-1}	17
Poly-PNBTH	1 mA cm^{-2}	413.2 F cm^{-3}	18
Poly(Zn-mTCPP)	5 A g^{-1}	142 F g^{-1}	19
p(Py-co-Cz)/MnO_x	5 A g^{-1}	352 F g^{-1}	20
p-TCTA	**15.1 A g^{-1}**	**347.8 F g^{-1} (349.8 F cm^{-3})**	**This Work**

4.3 Electrochemical cycling stability of p-TCTA

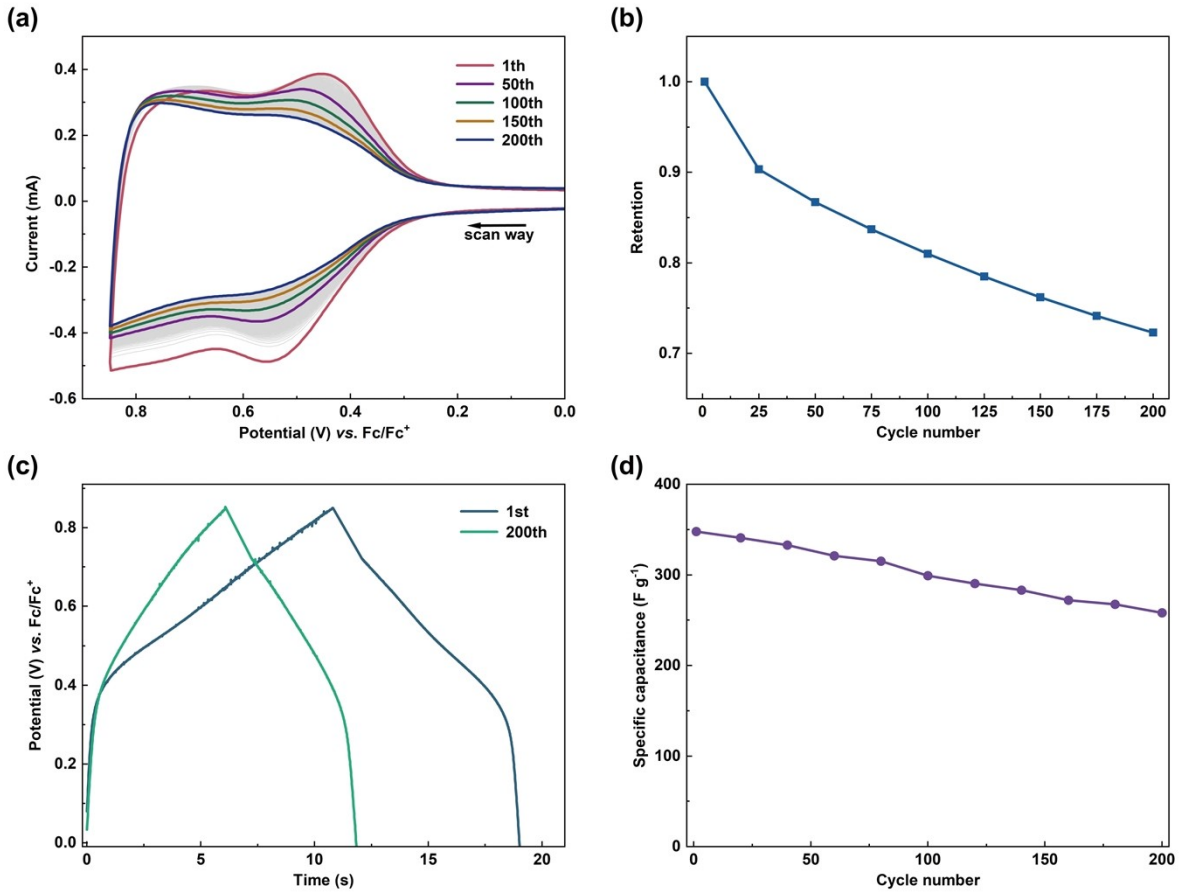

Fig. S10 (a) Cycling stability test of p-TCTA film measured by the CV method. (b) Retention of CV response as a function of cycle number. (c) Comparison between the first-cycle and the 200th-cycle GCD curve of p-TCTA. (d) Variation of specific capacitance with the number of GCD cycles. CV conditions, 0.1 M TBAPF6 in DCM/ACN/PC (2.5:0.6:1.9, v/v/v), potential window: 0-0.85 V, scan rate: 0.1 V s^{-1}. GCD conditions, 0.1 M TBAPF6 in DCM/ACN/PC (2.5:0.6:1.9, v/v/v), potential window: 0-0.85 V, current density: 15.1 A g^{-1}.

The cycling stability of p-TCTA films deposited on carbon paper was examined using both CV and GCD methods. As shown in Fig. S10, the film retained 72.3% of its initial CV response after 200 cycles. Similarly, after 200 charge-discharge cycles, the specific capacitance decreased to 74.2% of its initial value. These results indicate that the p-TCTA film exhibits moderate electrochemical cycling stability.

4.4 p-TCTA|PBFDO supercapacitor

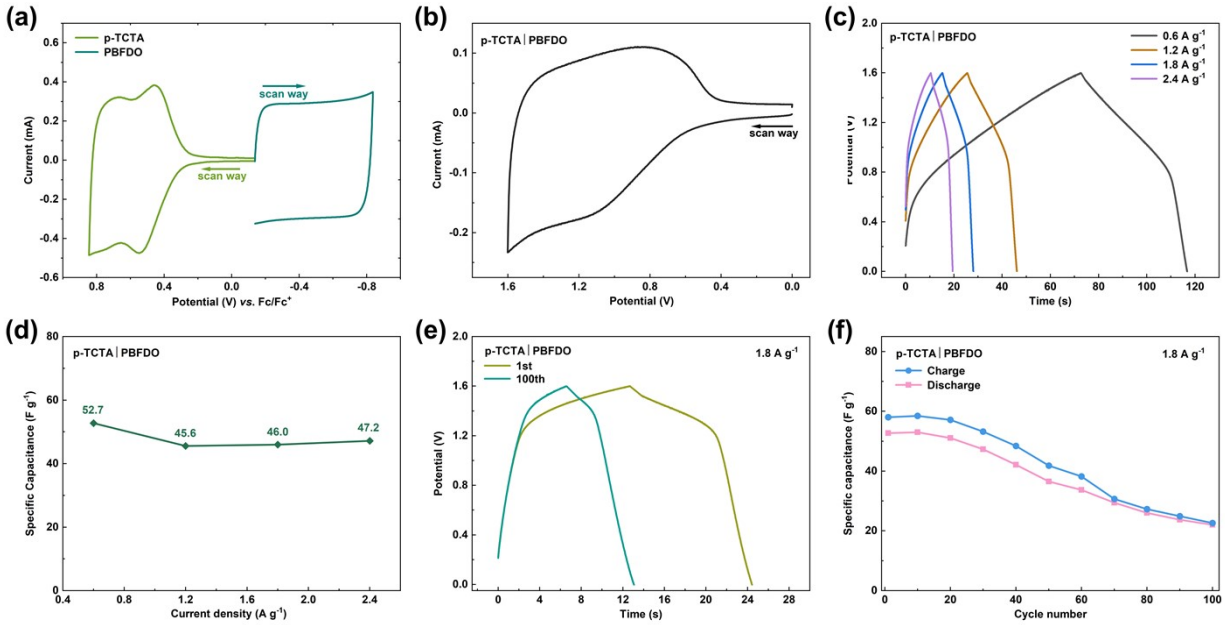

Fig. S11 (a) CV curves of p-TCTA and PBFDO electrodes. Electrochemical performance of the p-TCTA|PBFDO supercapacitor: (b) CV curves of the assembled device with a voltage window of 0-1.6 V; (c) GCD profiles of the device at various current densities; (d) specific capacitance of the device as a function of current density; (e) comparison between the first-cycle CV and the 100th-cycle GCD curve of the supercapacitor; (f) variation of the specific capacitance with GCD cycle number.

A p-TCTA|PBFDO asymmetric supercapacitor was fabricated to further characterize the capacitive performance of p-TCTA.[21,22] The positive electrode was prepared by depositing p-TCTA onto carbon paper, with an active material loading of approximately 0.007 mg cm^{-2}. For the negative electrode, a dimethylacetamide solution of PBFDO was diluted to 2 mg mL^{-1} and uniformly drop-cast (43 µL) onto pre-treated carbon paper (2 × 2 cm). The coated electrode was then dried under vacuum at 80 °C for 12 hours, resulting in a PBFDO-loaded electrode with an active material loading of 0.032 mg cm^{-2}.

The mass ratio of active materials for the positive and negative electrodes was matched based on charge balance calculations. The same electrolyte used in the three-electrode tests was employed here, and the two electrodes were assembled into an asymmetric supercapacitor. As shown in Fig. S11a and b, the CV curves of the individual electrodes and the assembled p-TCTA|PBFDO device demonstrate that the operating voltage window can reach up to 1.6 V. The GCD profiles of the p-TCTA|PBFDO device revealed a maximum discharge-specific capacitance of 52.7 F g^{-1} and a maximum charge-specific capacitance of 58 F g^{-1}. Multi-cycle GCD tests showed that after 100 charge-discharge cycles, the device retained 41.7% of its initial discharge capacitance and 39.0% of its charge capacitance.

5. SCLC measurements of p-TCTA

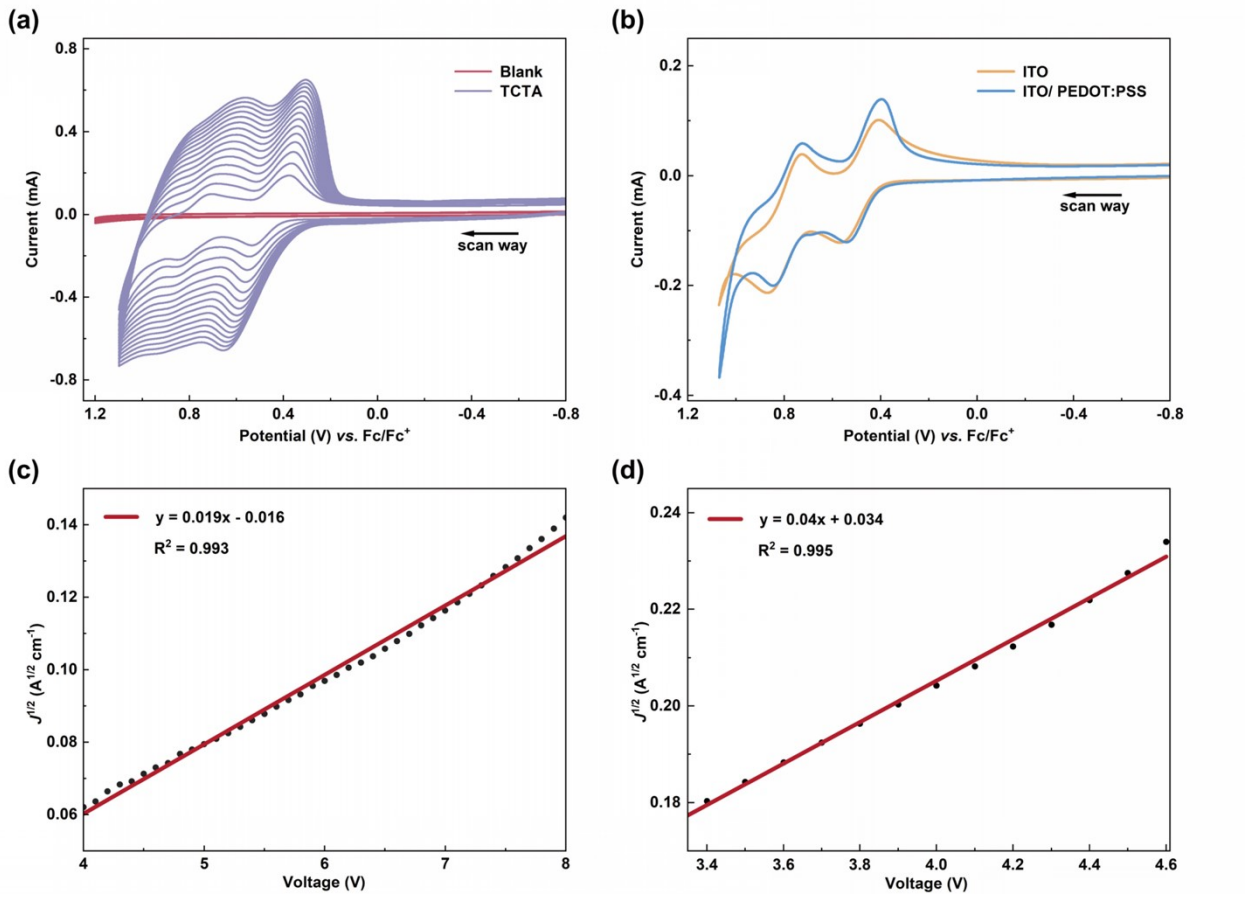

Fig. S12 (a) CV curves of TCTA electropolymerization on ITO/PEDOT:PSS, compared with CV curves of ITO/PEDOT:PSS in a monomer-free electrolyte, demonstrating the feasibility of TCTA electrodeposition on ITO/PEDOT:PSS. (b) Comparison of CV curves for TCTA electropolymerization on ITO and ITO/PEDOT:PSS substrates. (c) Detailed SCLC fitting corresponding to Fig. 3a. (d) Detailed SCLC fitting corresponding to Fig. 3b.

6. Spectroelectrochemistry of p-TCTA

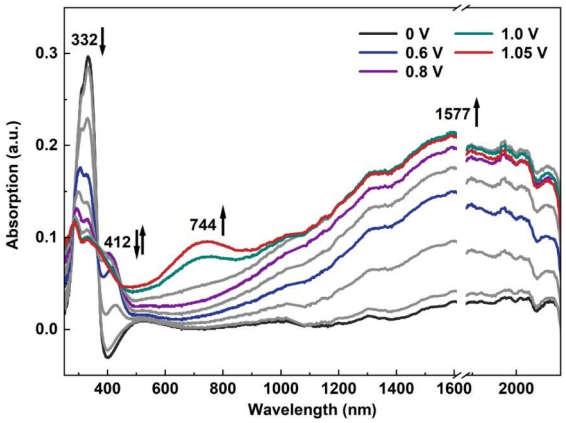

Fig. S13 Spectroelectrochemistry of p-TCTA.

7. Spectral characteristics of transitions between two species

Consider a reaction system involving only the interconversion between two species, α and β (e.g., the oxidation of species β to species α). The total concentration of the two species in the system remains constant, as described by Equation (3):

$$c_\alpha + c_\beta = c_0 \#(3)$$

Now, consider the absorbance $A(\lambda_1)$ at a given wavelength λ_1. By applying the Beer-Lambert law in conjunction with Equation (3), we obtain:

$$A(\lambda_1) = \varepsilon_{1,\ \alpha} c_\alpha l + \varepsilon_{1,\beta} c_\beta l = \varepsilon_{1,\beta} c_0 l + (\varepsilon_{1,\ \alpha} - \varepsilon_{1,\beta}) c_\alpha l \#(4)$$

Here, $\varepsilon_{1,\ \alpha}$ and $\varepsilon_{1,\beta}$ denote the molar extinction coefficients of species α and β at wavelength λ_1, respectively, and l represents the optical path length. A straightforward rearrangement of Equation (4) yields:

$$\Delta A(\lambda_1) = A(\lambda_1) - \varepsilon_{1,\beta} c_0 l = (\varepsilon_{1,\ \alpha} - \varepsilon_{1,\beta}) c_\alpha l \#(5)$$

If the spectrum of the system containing only species β is used as the initial reference spectrum, $\Delta A(\lambda_1)$ represents the difference between the absorbance at wavelength λ_1 in a specific state of the system and the initial spectrum. Similarly, for another wavelength λ_2, Equations (6) and (7) hold:

$$A(\lambda_2) = \varepsilon_{2,\ \alpha} c_\alpha l + \varepsilon_{2,\beta} c_\beta l = \varepsilon_{2,\beta} c_0 l + (\varepsilon_{2,\ \alpha} - \varepsilon_{2,\beta}) c_\alpha l \#(6)$$

$$\Delta A(\lambda_2) = A(\lambda_2) - \varepsilon_{2,\beta} c_0 l = (\varepsilon_{2,\ \alpha} - \varepsilon_{2,\beta}) c_\alpha l \#(7)$$

Combining Equations (5) and (7) results in:

$$\Delta A(\lambda_1) = \frac{(\varepsilon_{1,\ \alpha} - \varepsilon_{1,\beta})}{(\varepsilon_{2,\ \alpha} - \varepsilon_{2,\beta})} \times \Delta A(\lambda_2) \#(8)$$

The coefficients in Equation (8) are constants derived from the molar extinction coefficients of the two species. Consequently, for a system involving only the interconversion between two species, a key characteristic is that ΔA values at any two wavelengths exhibit a proportional relationship. While the above analysis is based on solution systems, the same conclusion holds true for film systems.

8. Refractive index and molecular number density

The correlation between film density and refractive index can be qualitatively evaluated using the Lorentz-Lorentz equation[23,24]

$$n^2 = 1 + 4\pi\chi \#(9)$$

$$\chi = \frac{N\alpha'}{1-\left(\frac{4\pi}{3}\right)N\alpha'} \#(10)$$

Here, *n* represents the refractive index of the film, *N* denotes the molecular number density (the number of molecules per unit volume), which reflects the film's compactness, and α' is the molecular polarizability volume. For a given material, the polarizability volume remains constant, establishing a positive correlation between *N* and *n*. Thus, the density of the film is positively correlated with its refractive index.

p-TCTA, as a crosslinked network of conjugated oligomeric segments linked by non-conjugated connections, exhibits decoupling between its conjugated segments. It is reasonable to assume that the polarizability volume of these segments is similar to that of the TCTA precursor. Under this assumption, the density of TCTA films produced via electrodeposition can be qualitatively compared to those produced by vapor deposition. Based on Fig. 4d, it can be concluded that the density of electrodeposited TCTA films is lower than that of vapor-deposited films.

9. The effect of torsional angles on charge transfer integrals between conjugated segments

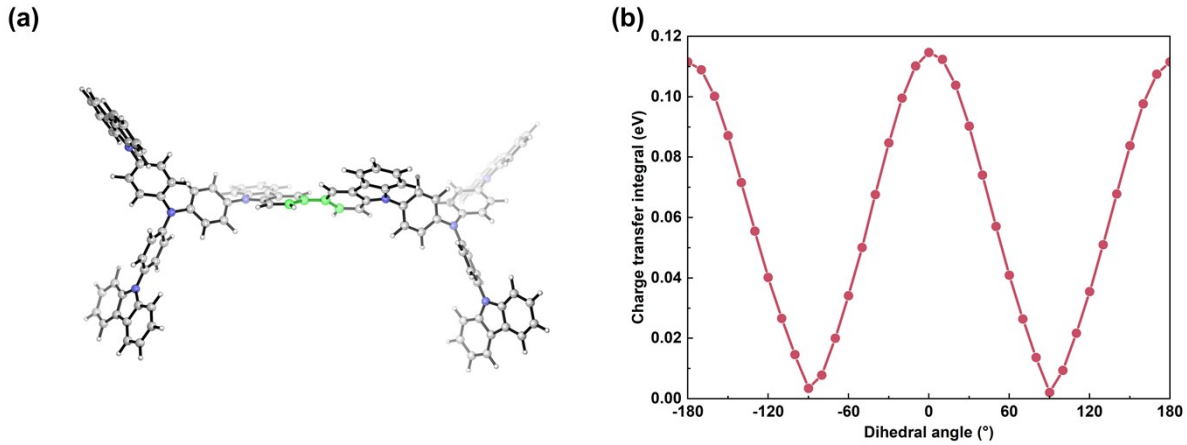

Fig. S14. (a) Optimized structure of p-TCTA dimeric model. (b) Calculated charge transfer integral (CTI) for dimeric model of p-TCTA as a function of inter-monomer torsion angle. This value provides an approximate quantitative measure of the electronic coupling between neighboring units.

In p-TCTA films, the charge transfer integral (CTI) between two coupled TCTA units reflects the strength of electronic coupling between conjugated segments and serves as an indicator of charge transfer capability. A dimeric model of p-TCTA was built to investigate the influence of inter-monomer torsion angles on the CTI. Geometric optimizations of ground states (DFT) was performed using PBE0-D3(BJ) functional.[25,26] The standard 6-311G(d,p) basis set[27,28] was used for all atoms. Harmonic vibration frequency calculations were performed for all stationary points to confirm them as a local minima. Geometric optimizations were carried out using Gaussian 16 programs.[29] The CTI between neighboring monomer can be defined as[30]:

$$|CTI| = \frac{1}{2}\sqrt{\left(E_{HOMO-1,full} - E_{HOMO,full}\right)^2 - \left(E_{HOMO,1} - E_{HOMO,2}\right)^2} \#(11)$$

where $E_{\text{HOMO-1,full}}$ and $E_{\text{HOMO,full}}$ are the orbital energies of the dimeric molecular model, and $E_{\text{HOMO,1}}$ and $E_{\text{HOMO,2}}$ are the HOMO energies of two H-atom-capping monomers at infinite separation. The optimized dimeric structure was visualized by CYLView program.[31]

Fig. S14a shows the optimized structure of the p-TCTA dimeric model, while Fig. S14b presents the calculated CTI of the p-TCTA dimer as a function of the inter-monomer torsion angle.It can be observed that the CTI reaches its maximum when the torsion angle is zero. As the torsion angle increases, the CTI gradually decreases, indicating reduced electronic coupling between the two TCTA units and a diminished degree of conjugation in the dimer. When the torsion angle reaches 90°, meaning the two units are oriented perpendicularly, the CTI attains its minimum value. These theoretical calculations clearly demonstrate that increased torsion between conjugated segments in p-TCTA reduces the film's charge transport capability.

10. Reaction schemes for charge transfer

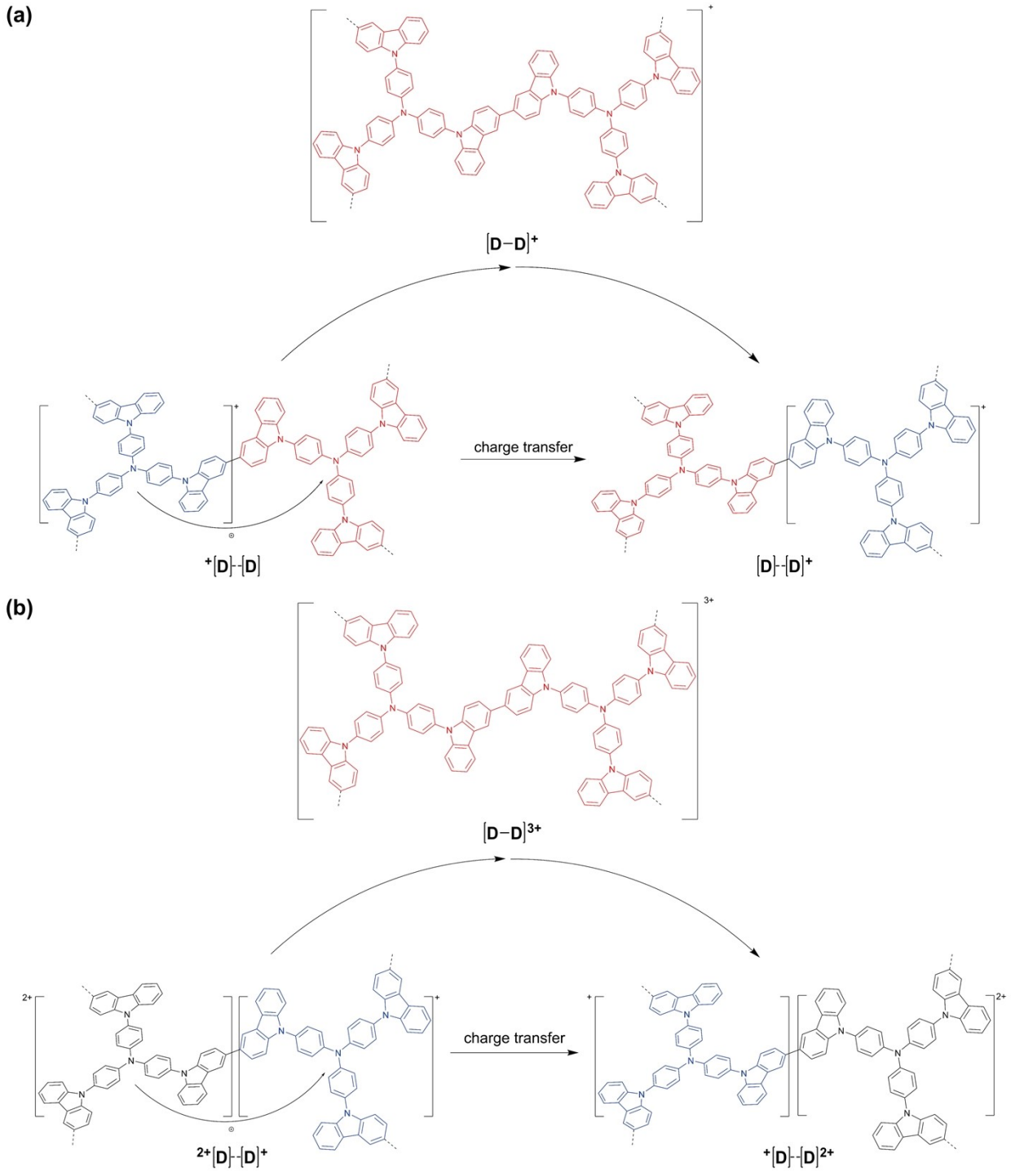

Fig. S15 Reaction schemes for charge transfer between conjugated fragments in (a) p-TCTA at low doping levels and (b) p-TCTA at high doping levels.

REFERENCES

1. A. G. Macedo, D. C. Silva, N. A. D. Yamamoto, L. Micaroni, R. M. Q. Mello and L. S. Roman, *Synth. Met.*, 2013, **170**, 63-68.
2. M. Innocenti, F. Loglio, L. Pigani, R. Seeber, F. Terzi and R. Udisti, *Electrochimica Acta*, 2005, **50**, 1497-1503.
3. E. Cha net and M. Billon, *J. Electroanal. Chem.*, 1998, **451**, 273-277.
4. J. Husson, S. Lakard, S. Monney, C. C. Buron and B. Lakard, *Synth. Met.*, 2016, **220**, 247-254.
5. E. Contal, S. Lakard, F. Dumur and B. Lakard, *Prog. Org. Coat.*, 2022, **162**, 106563.
6. E. C. Venancio, C. A. R. Costa, S. A. S. Machado and A. J. Motheo, *Electrochem. Commun.*, 2001, **3**, 229-233.
7. P. Tan, F. Lu and Y. Han, *Chem. Mater.*, 2023, **35**, 6024-6038.
8. E. Poverenov, M. Li, A. Bitler and M. Bendikov, *Chem. Mater.*, 2010, **22**, 4019-4025.
9. M. Li, S. Tang, F. Shen, M. Liu, W. Xie, H. Xia, L. Liu, L. Tian, Z. Xie, P. Lu, M. Hanif, D. Lu, G. Cheng and Y. Ma, *Chem. Commun.*, 2006, **32**, 3393-3395.
10. C. Gu, W. Dong, L. Yao, Y. Lv, Z. Zhang, D. Lu and Y. Ma, *Adv. Mater.*, 2012, **24**, 2413-2417.
11. C. Gu, T. Fei, M. Zhang, C. Li, D. Lu and Y. Ma, *Electrochem. Commun.*, 2010, **12**, 553-556.
12. A. J. Bard, L. R. Faulkner, In *Electrochemical Methods: Fundamentals and Applications*, John Wiley & Sons inc., Hoboken, 2nd ed, 2001, chapter 6th : Potential Sweep Methods, 226-246.
13. A. J. Bard, L. R. Faulkner, In *Electrochemical Methods: Fundamentals and Applications*, John Wiley & Sons inc., Hoboken, 2nd ed, 2001, chapter 5th : Basic Potential Step Methods, 210-214.
14. R. Rubio, M. B. Suarez, M. E. Pérez, D. A. Heredia, G. M. Morales, E. N. Durantini, L. Otero, M. Gervaldo and J. E. Durantini, *Electrochim. Acta*, 2023, **458**, 142552.
15. S. Topal, S. Topal, G. Suna, B. Ustamehmeto lu, T. Ozturk and E. Sezer, *Energy Technol.*, 2023, **11**, 2300015.
16. C. Zhang, Y. Xu, S. Sasaki and X. Wang, *Mater. Today Energy*, 2021, **21**, 100830.
17. C. Chen, Z. Zhu, X. Li and J. Li, *J. Appl. Polym. Sci.*, 2017, **134**, 44464.
18. X. Chen, W.-Y. Tung, K. Yang, Y.-M. Chen, K. Liu, C.-F. Cheng and Y. Zhu, *ACS Appl. Polym. Mater.*, 2019, **1**, 1634-1640.
19. H. Zhang, Y. Zhang, C. Gu and Y. Ma, *Adv. Energy Mater.*, 2015, **5**, 1402175.
20. E. Karaca, G. Özgenç, N. Ö. Pekmez and K. Pekmez, *J. Energy Storage*, 2022, **55**, 105794.
21. D. Ohayon, G. Quek, B. R. P. Yip, F. Lopez-Garcia, P. R. Ng, R. J. Vázquez, D. V. Andreeva, X. Wang and G. C. Bazan, *Adv. Mater.*, 2024, **36**, 2410512.
22. H. Zhang, M. Yao, J. Wei, Y. Zhang, S. Zhang, Y. Gao, J. Li, P. Lu, B. Yang and Y. Ma, *Adv. Energy Mater.*, 2017, **7**, 1701063.
23. S. S. Park, S. Lee, J. Y. Bae and F. Hagelberg, Phys. Lett., 2011, **511**, 466-470.
24. S. Lee, S. S. Park, and F. Hagelberg, Chem. Phys., 2012, **394**, 40-45.
25. C. Adamo, and V. Barone, *J. Chem. Phys.*, 1999, **110**, 6158-6170.
26. S. Grimme, S. Ehrlich, and L. Goerigk, *J. Comp. Chem.*, 2011, **32**, 1456-1465.
27. K. Raghavachari, J. S. Binkley, R. Seeger, and J. A. Pople, *J. Chem. Phys.*, 1980, **72**, 650-654.
28. T. Clark, J. Chandrasekhar and P. V. R. Schleyer, *J. Comp. Chem.*, 1983, **4**, 294-301.
29. Gaussian 16, Revision C.01, Frisch, M. J.; Trucks, G. W.; Schlegel, H. B.; Scuseria, G. E.; Robb, M. A.; Cheeseman, J. R.; Scalmani, G.; Barone, V.; Petersson, G. A.; Nakatsuji, H.; Li, X.; Caricato, M.; Marenich, A. V.; Bloino, J.; Janesko, B. G.; Gomperts, R.; Mennucci, B.; Hratchian, H. P.; Ortiz, J. V.; Izmaylov, A. F.; Sonnenberg, J. L.; Williams-Young, D.; Ding, F.; Lipparini, F.; Egidi, F.; Goings, J.; Peng, B.; Petrone, A.; Henderson, T.; Ranasinghe, D.; Zakrzewski, V. G.; Gao, J.; Rega, N.; Zheng, G.; Liang, W.; Hada, M.; Ehara, M.; Toyota, K.; Fukuda, R.; Hasegawa, J.; Ishida, M.; Nakajima, T.; Honda, Y.; Kitao, O.; Nakai, H.; Vreven, T.; Throssell, K.; Montgomery, J. A., Jr.; Peralta, J. E.; Ogliaro, F.; Bearpark, M. J.; Heyd, J. J.; Brothers, E. N.; Kudin, K. N.; Staroverov, V. N.; Keith, T. A.; Kobayashi, R.; Normand, J.; Raghavachari, K.; Rendell, A. P.; Burant, J. C.; Iyengar, S. S.; Tomasi, J.; Cossi, M.; Millam, J. M.; Klene, M.; Adamo, C.; Cammi, R.; Ochterski, J. W.; Martin, R. L.; Morokuma, K.; Farkas, O.; Foresman, J. B.; Fox, D. J. Gaussian, Inc., Wallingford CT, 2016.
30. S. B. Darling, *J. Phys. Chem. B*, 2008, **112**, 8891-8895.
31. CYLview, 1.0b; Legault, C. Y., Université de Sherbrooke, 2009 (http://www.cylview.org).